Automotive Science and Engineering, Vol. 14, No. 1, (2024), 4316-4326

Automotive Science and Engineering
Journal Homepage: ase.iust.ac.ir

ISSN: 2008-9899

Design and Static-Dynamic Analysis of a composites trailer chassis using failure theories

N. Taghizadeh [1], M. Esfahanian [2]

[1] Department of Mechanical Engineering, Isfahan University of Technology, Isfahan, Iran; taghizadehnasrollah@gmail.com

[2] Department of Mechanical Engineering, Isfahan University of Technology, Isfahan, Iran;

ARTICLE INFO

Article history:
Received : 10 Jan 2024
Accepted: 29 Feb 2024
Published: 16 Mar 2024

Keywords:
Composite
Trailer
Failure theories
Weight reduction

A B S T R A C T

Due to the importance of vehicle weight reduction which can reduce fuel consumption and air pollution, changes are made in vehicles. These changes can include changes in design, material, etc. In heavy trucks with payload limitation, the lighter trailers can provide higher load carrying capacity and more economical benefits. Composite materials are a good candidate for material exchange due to their resistance to various conditions and low weight compared to steel. In this paper, the trailer material made of steel will be replaced by composite so that strength density will remain the same. For this purpose, the finite element method is used for static and dynamic analyses. At first, the model of a two-axle trailer is developed using SolidWorks software. Then, using standard loading and failure theories (Tsai-Hill, Tsai-Wu), a number of composite layers and their suitable angles are selected for the chassis. Finally, static, modal, and dynamic analysis of the loaded trailer are performed using the finite element method with a composite material. Results show that 17 layers of polymer composite with glass fibers with 0-0 angle can reduce 17.7 percent weight.

1. Introduction

Chasses and car bodies contain the largest share of the total weight of the vehicles. This paper tries to reduce the weight by changing the chassis material from steel to composite in order to increase the bearing capacity and reduce greenhouse gases. In a previous study, Galos [1] researched on lightweight composite trailer design, in which he used composite panels to design the trailer chassis. Chandra [2] has modeled and analyzed the chassis of a heavy vehicle made of polymer composite with three different cross-sectional thicknesses. Siraj [3] has studied the static analysis of truck chassis frames made of composite materials. Liu [4] researched on Lightweight design of carbon twill weave fabric composite body structure for electric vehicle, Differences of the present study with previous works, is the use of Tsai-Hill and Tsai-Wu failure theories for appropriate modelling (select number of layers, select angles) for the trailer chassis.

2. Trailer chassis modeling

A chassis profile usually consists of longitudinal members with open and closed sections that are resistant to bending in the vertical direction. The members used in different areas of the trailer chassis have different shapes and dimensions. After measuring the dimensions and

*Corresponding Author
Email Address: mesf1964@iut.ac.ir
https://doi.org/10.22068/ase.2024.666

determining type of sections used in the chassis, a chassis model is developed in the SolidWorks. This chassis is a detachable ladder chassis and its characteristics are given in the table 1. [5]

Table 1-Steel chassis specifications[6]

capacity	36000kg
Width	24500mm
length	12350mm
Modulus Elasticity	207 GPa
Density	7800 kg/m3
Poisson Ratio	0.3
Yield Strength	550 MPa
Tensile Strength	620 MPa

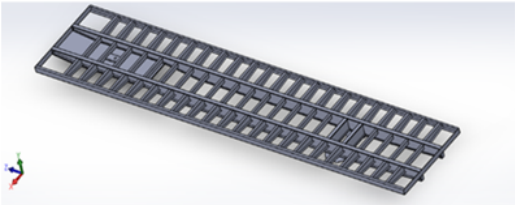

Fig 1. Developed model

THEORETICAL ANALYSIS

3. Tsai-Hill

The Tsai-Hill yield stress relationship includes the parameters G, H, F, L, M, and N which in the case of linear elastic behavior can be considered as a measure of rupture resistance as follows:

$$(\mathrm{G}+\mathrm{H})\sigma_1^2+(F+H)\sigma_2^2+(F+G)\sigma_3^2 - 2H\sigma_1\sigma_2-2G\sigma_1\sigma_3 - 2F\sigma_2\sigma_3+2L\tau_{23}^2+2M\tau_{13}^2 + 2N\tau_{12}^2=1 \quad (1)$$

The rupture parameters of the above relation can be calculated in terms of rupture resistances X, Y, S, Z for a layer.

If only the principal shear stress τ_{12} is applied to the body, given that this maximum shear stress can be equal to S, so: [7-9]

$$2N=\frac{1}{S^2} \quad (2)$$

Similarly, if the principal stress σ_1 is applied, the result is:

$$G+H=\frac{1}{X^2} \quad (3)$$

Where X is the maximum value of σ_1. If the stress σ_2 is applied with its maximum value of Y, the result is:

$$F+H=\frac{1}{Y^2} \quad (4)$$

Finally, if the stress σ_3 with its maximum value of Z is applied, the result is:

$$F+G=\frac{1}{Z^2} \quad (5)$$

The above coefficients can be calculated in terms of resistances.

$$2\mathrm{F}=\frac{1}{\mathrm{Y}^2}+\frac{1}{\mathrm{Z}^2}-\frac{1}{\mathrm{X}^2} \quad (6)$$

$$2\mathrm{G}=\frac{1}{X^2}+\frac{1}{Z^2}-\frac{1}{Y^2} \quad (7)$$

$$2H=\frac{1}{X^2}+\frac{1}{Y^2}-\frac{1}{Z^2} \quad (8)$$

For plane stress in plane (1-2) and for a monolayer in one direction, the values can be simplified to $\sigma_3=\tau_{13}=\tau_{23}=0$. It is also assumed that the resistance in direction 2 is equal the resistance in direction 3 and therefore Y = Z. Finally, the criterion of Tsai-Hill rupture is stated on the plane as follows.

$$\frac{\sigma_1^2}{X^2}+\frac{\sigma_1\sigma_2}{X^2}+\frac{\sigma_2^2}{Y^2}+\frac{\tau_{12}^2}{S^2}=1 \quad (9)$$

In the case of off-axis stress σ_x is defined using the following equation.

$$\sigma_1=\sigma_x cos^2\theta \quad (10)$$

$$\sigma_2=\sigma_x sin^2\theta \quad (11)$$

$$\tau_{12}=-\sigma_x sin\theta cos\theta \quad (12)$$

And as a result, the following relation is obtained.

$$\frac{cos^4\theta}{X^2}+\left(\frac{1}{S^2}-\frac{1}{X^2}\right)cos^2\theta sin^2\theta+\frac{sin^4\theta}{Y^2}=\frac{1}{\sigma_x^2} \quad (13)$$

4. Tsai-Wu

The Tsai-Wu criterion, another quadratic polynomial failure criterion that is more consistent with experimental results than Tsai-Hill, is expressed in a stress domain with six independent components as follows: [10-12]

$$\mathrm{f}_1\sigma_1+\mathrm{f}_2\sigma_2+\mathrm{f}_{11}\sigma_1^2+\mathrm{f}_{22}\sigma_2^2+\mathrm{f}_{66}\sigma_6^2-\sqrt{\mathrm{f}_{11}\mathrm{f}_{22}}\sigma_1\sigma_2=1 \quad (14)$$

$$\mathrm{f}_{11}=\frac{1}{\sigma_{11}^{\mathrm{T}}\sigma_{11}^{\mathrm{C}}} \quad (15)$$

$$\mathrm{f}_{22}=\frac{1}{\sigma_{22}^{\mathrm{T}}\sigma_{22}^{\mathrm{C}}} \quad (16)$$

$$\mathrm{f}_1=\frac{1}{\sigma_{11}^{\mathrm{T}}+\sigma_{11}^{\mathrm{C}}} \quad (17)$$

$$\mathrm{f}_2=\frac{1}{\sigma_{22}^{\mathrm{T}}+\sigma_{22}^{\mathrm{C}}} \quad (18)$$

$$\mathrm{f}_{66}=\left(\frac{1}{\sigma_{12}^{\mathrm{F}}}\right)^2 \quad (19)$$

$$.\mathrm{f}_{12}=-\left(\frac{1}{\sigma_y}\right)^2 \quad (20)$$

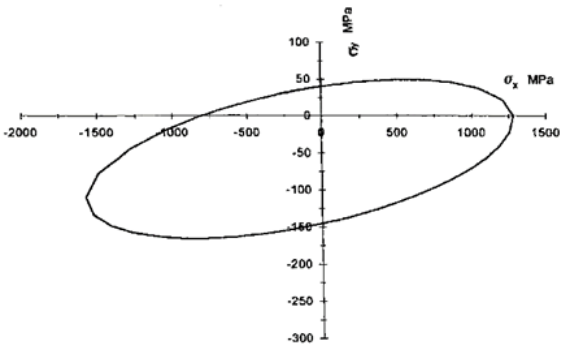

Fig 2. Tsai-Wu criterion in terms of plate tension [13]

5. Static analysis

The following formulation is used in static analysis.

$$[k]\{u\}=\{f^a\}+\{f^r\} \quad (21)$$

where $\{f^a\}$ is the vector of generally applied forces and $\{f^r\}$ is the vector of reaction force and $\{u\}$ is the vector of displacement of the node and $[k]$ is the stiffness matrix of the structure, which is defined as:

$$[k]=\sum_{m=1}^{n}[k_e] \quad (22)$$

Where $[k_e]$ is the stiffness matrix of the element and n is the number of elements.

$\{f^a\}$ is the vector of general applied forces, which is defined as:

$$\{\mathrm{f}^{\mathrm{a}}\}=\{\mathrm{f}^{\mathrm{nd}}\}+\{\mathrm{f}^{\mathrm{ac}}\}+\sum_{\mathrm{m}=1}^{\mathrm{N}}\left(\{\mathrm{f}_{\mathrm{e}}^{\mathrm{th}}\}+\{\mathrm{f}_{\mathrm{e}}^{\mathrm{pr}}\}\right) \quad (23)$$

In this equation (23) $\{f^{nd}\}$ is the load vector applied to the node, and $\{f^{ac}\}$ is the force vector due to gravity, $\{f_e^{th}\}$ is the thermal force vector of the element, and $\{f_e^{pr}\}$ is the compressive force vector of the element.

$[f^{ac}]$ is The force vector due to the point of gravity, which can be defined as:

$$[f^{ac}]=-[M]\{a_c] \quad (24)$$

In this equation (24), $\{a_c]$ is the total acceleration vector of the structure and $[M]$ is the total mass matrix of the structure, which is defined as:

$$[M]=\sum_{m=1}^{N}[M_e] \quad (25)$$

$[M_e]$ is the element mass matrix.[14]

6- Modal analysis

The equation of motion of a non-damped system will defined be as follows. [15]

$$[M]\{\ddot{u}\} + [k]\{u\} = \{\cdot\} \quad (26)$$

Free vibrations are a linear system in the following harmonic form:

$$\{u\} = \{\varphi_i\} cos\omega_i t \quad (27)$$

In this equation (27) $\{\varphi_i\}$ is a special vector, ω_i is the frequency of the circle and t is the time.

We have the above two equations (26 & 27) by merging:

$$(-\omega_i^2[M] + [k])\{\varphi_i\} = \{0\} \quad (28)$$

Equation (28) has two categories of answers. The first case $\{\varphi_i\} = \{0\}$ which has a real answer and the second case $(-\omega_i^2[M] + [k]) = \{0\}$ which has an imaginary answer and can be written as follows.

$$f_i = \frac{\omega_i}{2\pi} \quad (29)$$

in this relation f_i, is the natural frequency.

7. Dynamic analysis

The transient dynamic equilibrium equation for a structure is given as [16, 17] :

$$[M]\{\ddot{u}\} + [C]\{\dot{u}\} + [K]\{u\} = \{F^a\} \quad (30)$$

Where $[M]$ is a mass matrix, $[C]$ is the damping matrix, $[K]$ is the stiffness matrix, $\{\ddot{u}\}$ acceleration vector, $\{\dot{u}\}$ velocity vector, $\{u\}$ displacement vector and $\{F^a\}$ is the applied load vector. In this case, all points of the structure move with the same known frequency.

For different phase angles, the displacements are defined as:

$$\{u\} = \{u_{max} e^{i\emptyset}\} e^{i\Omega t} \quad (31)$$

where u_{max} is the maximum displacement and $\Omega = 2\Pi f$ is the circular frequency, (t) is time and ϕ is phase angle.

The equation is rewritten as:

$$\{u\} = \{u_{max}(cos\phi + i\, sin\phi)\} e^{i\Omega t} \quad (32)$$

$$\{u\} = (\{u_1\} + i\{u_2\}) e^{i\Omega t} \quad (33)$$

where $\{u_1\} = (\{u_{max} cos\phi\}$ and $\{u_2\} = \{u_{max} sin\phi\}$ are real and imaginary displacement vectors, respectively.

Similarly, the force vector can be defined as:

$$\{F\} = \{F_{max} e^{i\psi}\} e^{i\Omega t} \quad (34)$$

$$\{F\} = \{F_{max}(cos\psi + i\, sin\psi)\} e^{i\Omega t} \quad (35)$$

$$\{F\} = (\{F_i\} + i\{F_2\}) e^{i\Omega t} \quad (36)$$

By placing the displacement relations, we will have where F_{max} is the force amplitude, and ψ is the angle of the force phase. $(-\Omega^2\{M\} + i\Omega\{c\} + \{K\})(\{u_1\} + i\{u_2\}) e^{i\Omega t} = (\{F_1\} + i\{F_2\})$ (37)

By removing $e^{i\Omega t}$ from both sides we have:

$$([K] - \Omega^2[M] + i\Omega[c])(\{u_1\} + i\{u_2\}) = \{F_1\} + i\{F_2\} \quad (38)$$

Dynamic excitation occurs at the wheel-to-road contact point when the vehicle passes through a rough road.

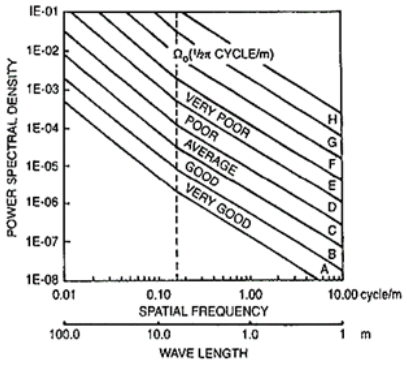

Fig 3. Road classification[18]

When the wheels on both sides pass over the same obstacle, movements resulting from symmetrical excitation are applied to the chassis. These excitations are applied to the wheels in three types: speed bump, pit, and obstacle.

7-1 Speed bump, Obstacle, Pit

The excitation is assumed to have a height of 10 cm. Pictures 4 to 6 depict these excitations. They are defined according to the standard speed of 40 km/h and a width of 4.7 meters for each excitation, resulting in a duration of 0.43 seconds for each wheel. The distance between the two excitations is determined to be 0.45 seconds based on the wheelbase and the vehicle's speed.

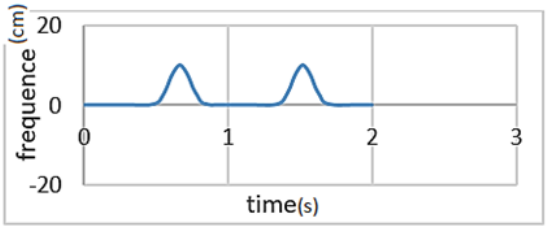

Fig 4. Displacement diagram for speed bump excitation.

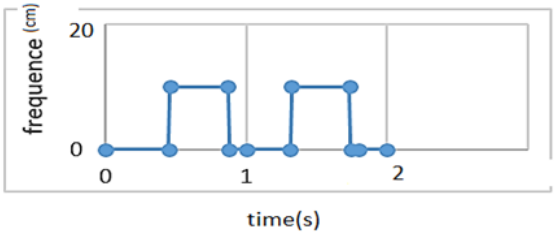

Fig 5. Displacement diagram for obstacle excitation.

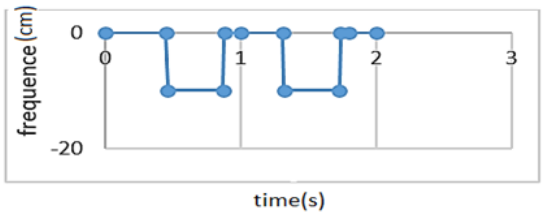

Fig 6. Displacement diagram for pit excitation

Discussion

8. Composite used in chassis

Polymer composite with glass fibers has been utilized for the chassis material in the present paper. Within the developed model, two types of Woven Roving (WR) fibers and Continuous Strand Mat (CSM) fibers have been employed. Woven Roving fibers (table 2) are allocated to the first and last layers due to their excellent adhesion properties, which help preserve the resin. Continuous Strand Mat fibers (table 3) are incorporated into the layers in the middle to enhance the composite's strength against applied loads.

Vinyl ester resin is chosen for this model due to its advantageous characteristics, including good mechanical and chemical properties, as well as outstanding corrosion resistance.

Table 2-Typical mechanical properties of FRP laminate CSM [19]

Fiber volume fraction V_f	0.18
Specific gravity	1.5
Yang's Modul	8 GPa
Shear modulus	3 GPa
Poisson's ratio	0.3 GPa
Tensile strength σ_{UT}	100 MPa
Compressive strength	140 MPa
Shear strength	75 MPa
Specific Young's modulus	5.3 E/SG
Specific tensile strength	67 σ_{UT}/SG
Density	1.44 g/cm^3

Table 3-Typical mechanical properties of FRP laminate WR [19]

Fiber volume fraction Vf	0.34
Specific gravity	1.7
Yang's Modul	15 GPa
Shear modulus	3.5 GPa
Poisson's ratio	0.3 GPa
Tensile strength σ_{UT}	250 MPa
Compressive strength	210 MPa
Shear strength	100 MPa
Specific Young's modulus	8.8 E/SG
Specific tensile strength	147 σ_{UT}/SG
Density	1.63 g/cm^3

In the composite utilized for the chassis, the selection of the number of layers and fiber angles should be conducted to achieve the highest resistance with the least number of layers. To determine this number of layers and fiber angles, the static analysis of the chassis should be conducted. Initially, a hypothetical selection of a 5-layer composite with two different fiber angles, 0-0 and 0-90, is made, as depicted in Fig 7 and 8. Subsequently, employing boundary conditions and standard loading, static analysis of the chassis is conducted, and the Tsai-Hill and Tsai-Wu criteria are obtained and depicted in Fig 9 to 12.

For 5 layers of composite with fiber angles of 0 - 90 degrees, the maximum Tsai-Hill value is found to be 11.51, and the maximum Tsai-Wu value is 12.80. For 0 - 0 angles, the maximum Tsai-Hill value is 10.91, and the maximum Tsai-Wu value is 14.62.

As previously mentioned, for optimal results, the values of Tsai-Hill and Tsai-Wu should be close to or near one. Therefore, the results for 5 composite layers are deemed unsatisfactory, and consequently, the analysis is repeated by including an additional layer with a suitable angle. Results for the six-layer composite are presented in Fig 13-18.

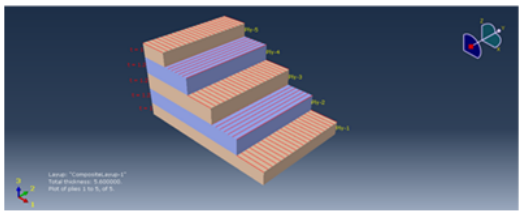

Fig 7. 5 layers 0 - 90 arrangement

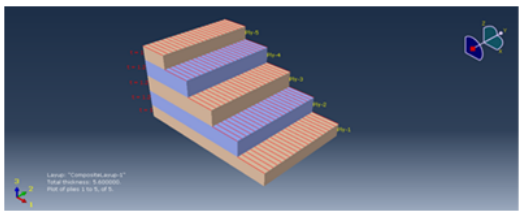

Fig 8. 5 layers 0 - 0 arrangement

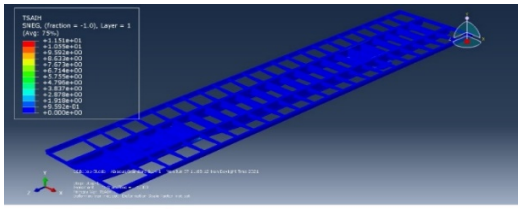

Fig 9. Tsai-Hill for 0 - 90 in 5 layers arrangement

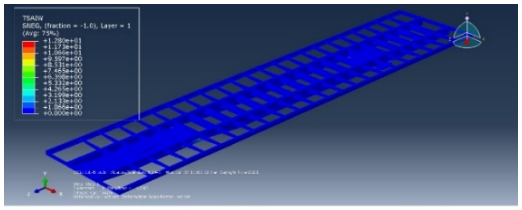

Fig 10. Tsai-Wu for 0 - 90 in 5 layers arrangement

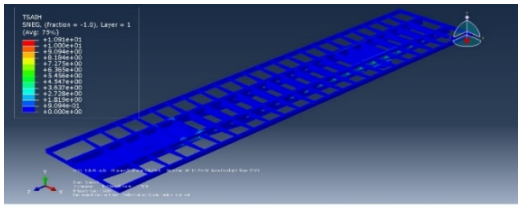

Fig 11. Tsai-Hill for 0 - 0 in 5 layers arrangement

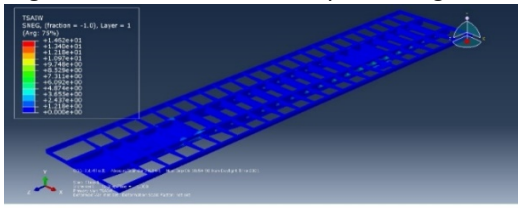

Fig 12. Tsai-Wu for 0 - 0 in 5 layers arrangement

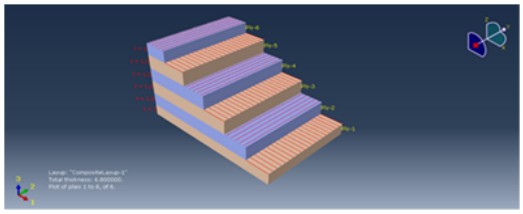

Fig 13. 6 layers 0 - 90 arrangement

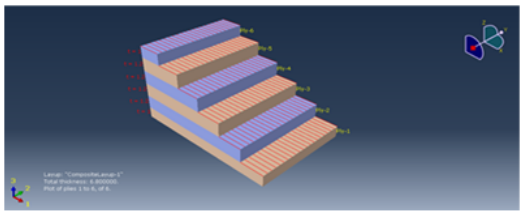

Fig 14. 6 layers 0 - 0 arrangement

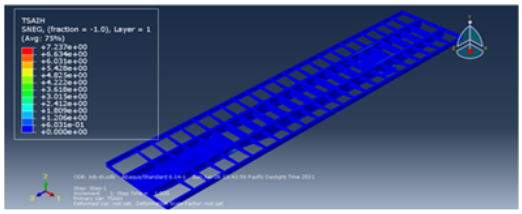

Fig 15. Tsai-Hill for 0 - 90 in 6 layers arrangement

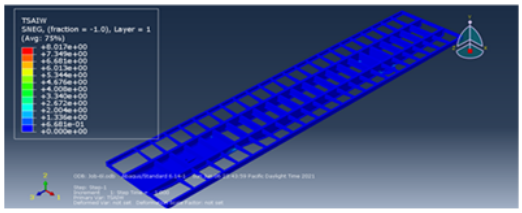

Fig 16. Tsai-Wu for 0 - 90 in 6 layers arrangement

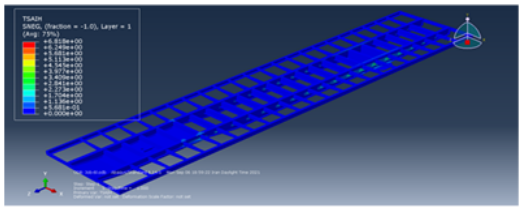

Fig 17. Tsai-Hill for 0 - 0 in 6 layers arrangement

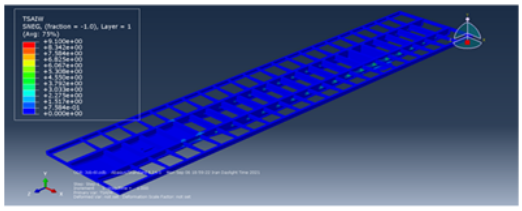

Fig 18. Tsai-Wu for 0 - 0 in 6 layers arrangement

After analysis and obtaining the results for 6 layers with 0-90 degree fiber angles, the maximum Tsai-Hill value becomes equal to 7.23 and the maximum Tsai-Wu value is equal to 8.01. Similarly, for 0-0 fiber angles, the maximum Tsai-Hill value equals 6.81 and the maximum Tsai-Wu value equals 9.10. Once again, these values are not considered fitting for Tsai-Hill and Tsai-Wu criteria. However, compared with the results for 5 layers, there is a reduction in Tsai-Hill and Tsai-Wu values, which improves the situation. To address this, a layer with a suitable angle is added, and the analysis is repeated. The results are presented in Table 4..

Table 4-Refractive index for the number of porcelain layers and different angles

Number of layers	$(\text{Tsai-Hill})_{max}$ for 0 - 90 angle	$(\text{Tsai-wu})_{max}$ for 0 - 90 angle	$(\text{Tsai-Hill})_{max}$ for 0 - 0 angle	$(\text{Tsai-wu})_{max}$ for 0 - 0 angle
5	11.51	12.80	10.91	14.62
6	7.23	8.01	6.81	9.10
7	4.90	5.24	4.50	6.18
9	2.91	3.41	2.82	3.67
10	2.29	2.71	2.20	2.85
11	1.91	2.27	1.79	2.31
12	1.62	1.94	1.49	1.92
14	1.36	1.61	1.22	1.53
15	1.20	1.40	1.06	1.30
16	1.08	1.23	0.93	1.13
17	0.95	1.09	0.83	1.00
18	0.86	0.98	0.61	0.64

The values of Tsai-Wu and Tsai-Hill are expected to be close to 1. Table 4 illustrates that for 17 layers with 0 - 90 fiber angles, the value of Tsai-Wu is 1.09 and the value of Tsai-Hill is 0.95. For 17 layers with 0 – 0 fiber angles, these values are 1 and 0.83, respectively. Therefore, due to the lower values for 0 - 0 fiber angles compared to those of 0 – 90, the 17-layer composite with 0 – 0 fiber angle is selected in the present paper.

9- Chassis Static analysis

In the static analysis of the chassis, the maximum payload that can be carried by the trailer is regarded as the load, and the chassis is capable of displacing in the direction of the springs.

In this section, the chassis is statically analyzed using the finite element method with Abacus software. Fig 19 depicts the static analysis results for the steel chassis, with the maximum Von-Mises stress recorded at 68.45 MPa. Similarly, for the 17-layer composite chassis, as shown in Fig 19, the maximum Von-Mises stress is measured at 37.18 MPa.

10-Chassis modal analysis

The first eight modes of chassis vibration are obtained numerically and are depicted in figures 20 to 27 and table 5.

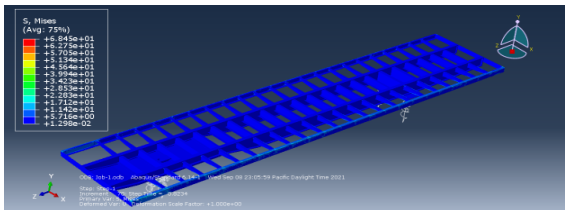

Fig 19. Steel Chassis Static analysis

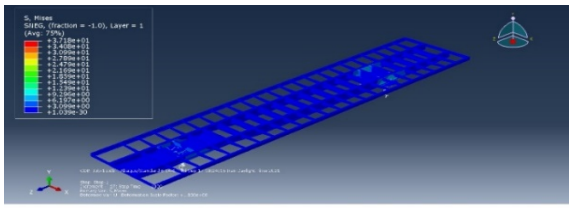

Fig 20. Composite chassis Static analysis

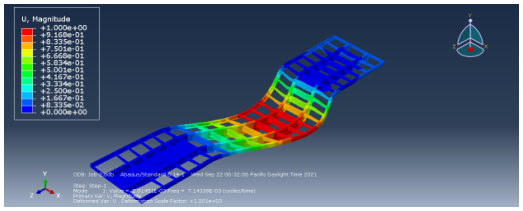

Fig 20. The first vibrating mode of the chassis

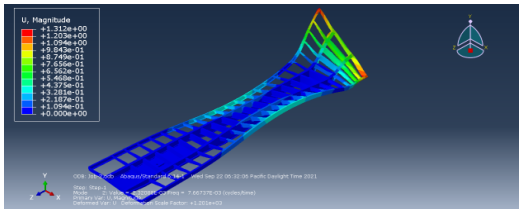

Fig 21. The second vibrating mode of the chassis

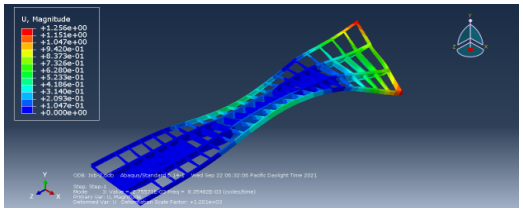

Fig 22. The third vibrating mode of the chassis

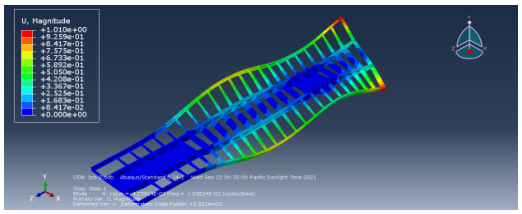

Fig 23. The fourth vibrating mode of the chassis

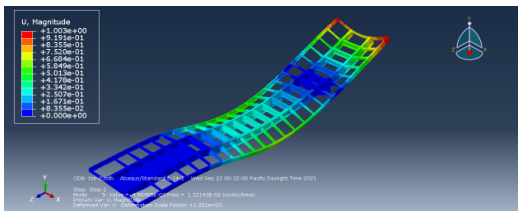

Fig 24. The fifth vibrating mode of the chassis

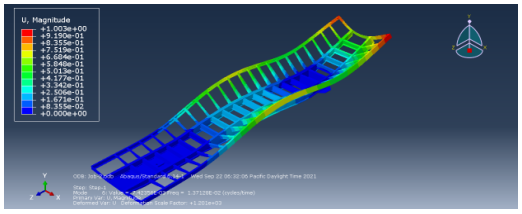

Fig 25. The sixth vibrating mode of the chassis

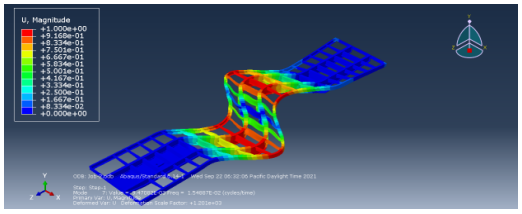

Fig 26. The seventh vibrating mode of the chassis

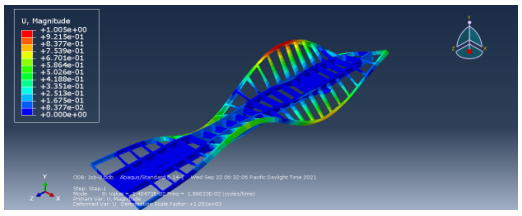

Fig 27. The eighth vibrating mode of the chassis

Table 6 presents the natural frequencies related to the first 8 modes of vibration for the steel chassis. The results indicate a favorable comparison with the natural frequencies of a steel chassis provided by Agrawal [18]

Table 5-The first eight composite chassis vibration modes

Mode Shape	Natural frequency
1	7.1 433
2	7.6673
3	8.3548
4	10.3624
5	11.2143
6	13.7128
7	15.4887
8	18.8633

Table 6-The first eight steel chassis vibration modes

Mode Shape	Natural frequency	
	Present work	Reference work[15]
1	16.746	16.894
2	18.719	25.537
3	33.388	27.427
4	36.667	28.746
5	37.096	33.971
6	43.202	34.316
7	47.389	36.564
8	62.701	46.316

11-Chassis dynamic analysis

This section addresses the dynamic analysis of the chassis. Displacement excitations, including pit hole, speed bump, and obstacle, are utilized for the wheels. Initially, these excitations are applied to the front axle and then with a time lag to the rear axle. The effect of these displacement excitations on the stress generated in the chassis is subsequently investigated.

In the dynamic analysis, a static payload is applied to the chassis, followed by the addition of the load resulting from road excitation. Therefore, the overall stresses encompass those due to static and dynamic loads.

12-Stimulation of the speed bump

Two displacement excitations, with a time interval specified in Figure (4), are applied to the front and rear wheels, and the effect of these displacements on the stresses generated in the chassis is investigated. As depicted in Fig 28, the maximum Von-Mises stress is generated at the rear axle, with a value of 165.5 MPa. The same simulation for the steel chassis results in a maximum Von-Mises stress of 177.1 MPa.

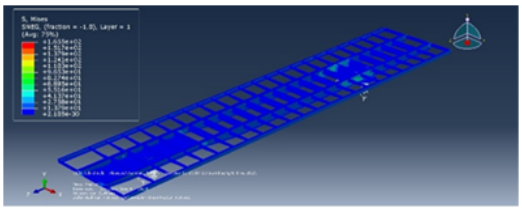

Fig 28. Composite chassis dynamic analysis with speed bump excitation

Stimulation of the obstacle

Two displacements, with a time interval specified in Fig (5), are initially applied to the front axle suspension and subsequently to the rear axle suspension, and the effect of this displacement on the stresses generated in the chassis is investigated. As depicted in Fig 29, the maximum Von-Mises stress occurs near the front axle, with a value of 183 MPa. This value for the steel chassis is 244.2 MPa.

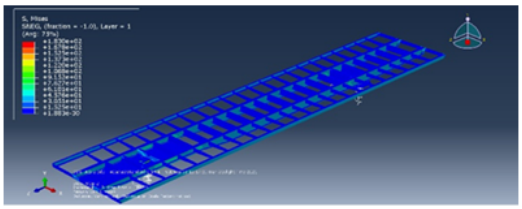

Fig 29. Composite chassis Dynamic analysis with obstacle excitation

Stimulation of the pit hole

Two displacements, with a specified time interval as shown in Figure (6), are initially applied to the front axle suspension and subsequently to the rear axle suspension. The effect of this excitation on the stresses generated in the chassis is depicted in Fig 30. The maximum Von-Mises stress is observed near the rear axle, with a value of 107.8 MPa. For the steel chassis, the maximum Von-Mises stress is 141.6 MPa.

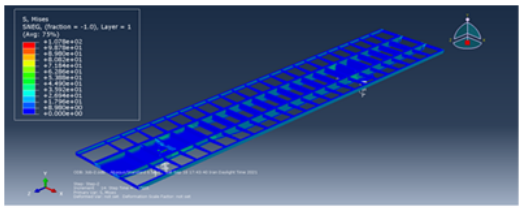

Fig 30. Composite chassis dynamic analysis with hole excitation

By comparing the maximum Von-Mises stresses for steel and composite chassis, the stresses that occur in the composite chassis are much smaller due to the increase in the thickness of the composite structure.

13-Conclusion

The purpose of this study is to reduce the weight of the trailer by changing its material from steel to composite. The identified optimal choice was the fiber glass polymer composite. Through the utilization of the failure theories of Tsai-Hill and Tsai-Wu, analysis has indicated that the arrangement of 17 layers of composite with a 0-0 angle provides the most favorable outcomes. Furthermore, static, modal, and dynamic analyses have been conducted on both steel and composite chassis.

The steel chassis has a mass of 3621 kg based on the steel density of 7800 kg/m³ [15]. The weight of the 17-layer composite chassis, calculated using the density provided in Tables 2 and 3, is 2979 kg. This results in a weight reduction of 642 kg. This weight reduction not only enhances the load capacity of the trailer but also contributes to reductions in fuel consumption and greenhouse gas emissions.

References

1. Galos, J.L., *Lightweight composite trailer design.* 2017, University of Cambridge.
2. Chandra, M.R., S. Sreenivasulu, and S.A. Hussain, *Modeling and Structural analysis of heavy vehicle chassis made of polymeric composite material by three different cross sections.* International Journal of Modern Engineering Research, 2012. **2**(4): p. 2594-2600.
3. Siraj, A., N.R. Babu, and K.S. Reddy, *Static analysis of dump truck chassis frame made of composite materials.* International Journal of Engineering, Science and Technology, 2019. **11**(2): p. 21-32.
4. Liu, Q., et al., *Lightweight design of carbon twill weave fabric composite body structure for electric vehicle.* Composite Structures, 2013. **97**: p. 231-238.
5. Kurdi, O. and R.A. Rahman, *Finite element analysis of road roughness effect on stress distribution of heavy duty truck chassis.* International journal of technology, 2010. **1**(1): p. 57-64.
6. Juvinall, R. and K. Marshek, *Fundamental Machine Component Design, John Willey & Son.* Inc., USA, 2006.
7. Arola, D. and M. Ramulu, *Orthogonal cutting of fiber-reinforced composites: A finite element analysis.* International Journal of Mechanical Sciences, 1997. **39**(5): p. 597-613.
8. Tsai, S.W., *Strength theories of filamentary structure.* Fundamental aspects of fiber reinforced plastic composites, 1968.
9. Cortés, P. and W.J. Cantwell, *The prediction of tensile failure in titanium-based thermoplastic fibre–metal laminates.* Composites Science and Technology, 2006. **66**(13): p. 2306-2316.
10. Frangopol, D.M. and S. Recek, *Reliability of fiber-reinforced composite laminate plates.* Probabilistic Engineering Mechanics, 2003. **18**(2): p. 119-137.
11. Wolfe, W.E. and T.S. Butalia, *A strain-energy based failure criterion for non-linear analysis of composite laminates subjected to biaxial loading.* Composites Science and Technology, 1998. **58**(7): p. 1107-1124.
12. Hyer, M.W. and S.R. White, *Stress analysis of fiber-reinforced composite*

materials. 2009: DEStech Publications, Inc.

13. Liu, K.-S. and S.W. Tsai, *Chapter 3.10 - A progressive quadratic failure criterion for a laminate**, in *Failure Criteria in Fibre-Reinforced-Polymer Composites*, M.J. Hinton, A.S. Kaddour, and P.D. Soden, Editors. 2004, Elsevier: Oxford. p. 334-352.
14. Wang, X. and H. Gu, *Static analysis of frame structures by the differential quadrature element method.* International Journal for Numerical Methods in Engineering, 1997. **40**(4): p. 759-772.
15. Agrawal, M.S. and M. Razik, *Finite element analysis of truck chassis frame*. International Research Journal of Engineering and Technology, 2015. **2**(3): p. 1949-1956.
16. Yang, Y.-B. and J.-D. Yau, *Vehicle-bridge interaction element for dynamic analysis.* Journal of Structural Engineering, 1997. **123**(11): p. 1512-1518.
17. Lu, X., C.-W. Kim, and K.-C. Chang, *Finite element analysis framework for dynamic vehicle-bridge interaction system based on ABAQUS.* International Journal of Structural Stability and Dynamics, 2020. **20**(03): p. 2050034.
18. Fermer, M., G. McInally, and G. Sandin. *Fatigue life analysis of Volvo S80 bi-fuel*. in *Proceedings of 1st MSC worldwide automotive conference, MSC*. 1999.
19. Shenoi, R.A. and J.F. Wellicome, *Composite Materials in Maritime Structures: Volume 2, Practical Considerations*. Vol. 2. 1993: Cambridge University Press.